

**SIMULATION ON PERFORMANCE OF GaN-BASED LIGHT EMITTING  
DIODES WITH VARIED GEOMETRY AND CONTACTS DESIGN**

**MUHAMMAD FIRDAUS BIN OTHMAN**

**2010**

**SIMULATION ON PERFORMANCE OF GaN-BASED LIGHT EMITTING  
DIODES WITH VARIED GEOMETRY AND CONTACTS DESIGN**

**by**

**MUHAMMAD FIRDAUS BIN OTHMAN**

**Thesis submitted in fulfillment of the requirements  
for the degree of  
Master of Science**

**JUNE 2010**

## ACKNOWLEDGEMENTS

First and foremost, I thank Allah the Almighty for His grace and blessings, for giving me strength and patience in order to finish my thesis. I also would like to express my gratitude to my main supervisor, Associate Prof. Dr. Azlan Abdul Aziz for his constant guidance, constructive encouragements and beneficial critics all the way through the supervision of my study. Special thank to my second supervisor, Associate Prof. Dr. Md. Roslan Hashim for his big help especially in term of consultation in simulation works. With a deep sense of honour, I express my gratitude to both of them for realizing my true abilities even though I felt like I was always far away from their expectations.

Besides, I also would like to thank all of the staff from Solid State Lab and Nano-Optoelectronics Research and Technology Laboratory (N.O.R) for their support. I gratefully acknowledge the contributions of my former and present colleagues, Dr. Sabah M. Thalhab, Mr. Mohd Zaki Yusuff, Mr. Nik Mohd Izham Mohamed Nor, Ms. Norzaini Zainal, Ms. Farah Liyana Mohamad Khir, Mr. Mohd Zamrus Ali, Ms. Siti Azlina Rosli and all of my lab mates for giving me moral support and keeping me accompanied through ups and downs of my study period.

Finally, my sincerest appreciation goes to my family and my beloved wife, Mrs. Nor Azliza Ismail for putting their faith in me and blessing the path that I chose. I appreciated for each of their sacrifices, patience and endless love showered to me throughout my life. Hopefully, this thesis will be regarded as a reward for all of the patience and sacrifices that had been made and become a stepping stone for the next level.

## TABLE OF CONTENTS

	Page
ACKNOWLEDGEMENTS	ii
TABLE OF CONTENTS	iii
LIST OF TABLE	vi
LIST OF FIGURES	vii
LIST OF SYMBOLS	xii
LIST OF ABBREVIATIONS	xiv
ABSTRAK	xv
ABSTRACT	xvii
CHAPTER 1 - INTRODUCTION	
1.1 Light Emitting Diode (LED)	1
1.2 Gallium Nitride (GaN) based LED	3
1.3 Geometrical design issues on lateral GaN-based LEDs performance	4
1.4 The advancement of simulation	11
1.5 The research objective	12
1.6 Outline of Thesis	13
CHAPTER 2 - THEORY	
2.1 Introduction	15
2.2 Principle of LED	15
2.3 Radiative and non-radiative recombinations	18
2.3.1 Radiative electron-hole recombination	20
2.3.2 Non-radiative electron-hole recombination	21
2.3.3 Competition between radiative and non-radiative recombination	25
2.4 Current crowding in LEDs on insulating substrates	26
2.5 Summary	34

## CHAPTER 3 - SIMULATION PROCEDURES

3.1	Introduction	35
3.2	ISE TCAD	35
3.2.1	MDRAW	36
3.2.2	DEVISE	36
3.2.3	MESH	37
3.2.4	DESSIS	39
3.2.4.1	Command file	40
3.2.4.2	Parameter file	43
3.2.5	INSPECT	43
3.2.6	TECPLOT	44
3.3	2D and 3D Simulation	47
3.4	Lateral LED structure	51
3.5	Summary	53

## CHAPTER 4 - EFFECTS OF LED CONTACT GEOMETRICS ON ITS PERFORMANCE

4.1	Introduction	54
4.2	Effects of lateral distance on LED performance	54
4.3	Effects of contact geometry on LED performance	64
4.4	Effects of contact size area on LED performance	74
4.5	Summary	78

## CHAPTER 5 - EFFECTS OF LED MESA SIDEWALL GEOMETRICS ON ITS PERFORMANCE

5.1	Introduction	80
5.2	Effects of slanted mesa sidewall on LED performance	80
5.3	Effects of lateral and vertical configurations on LED performance	93
5.4	Summary	103

CHAPTER 6 - CONCLUSION AND FUTURE WORK	
6.1 Conclusion	104
6.2 Future work	107
REFERENCES	109
APPENDICES	
LIST OF PUBLICATIONS & SEMINARS	

## **LIST OF TABLE**

**Page**

Table 3.1	The material parameters that are used in simulation work	<b>42</b>
-----------	--	-----------

<b>LIST OF FIGURES</b>		<b>Page</b>
Figure 1.1	Evolution of LED and organic LED (OLED) performance [Source: Sheats <i>et al.</i> , 1996].	<b>2</b>
Figure 1.2	The plane view of typical LED and modified LED. The dotted arrows in the LED show the possible path for uniform current spreading during LED performance. (a) the typical LED. (b) the modified LED with extra pad at p-type.	<b>7</b>
Figure 1.3	The geometry of interdigitated geometry LED.	<b>9</b>
Figure 1.4	The geometry of microring LED.	<b>10</b>
Figure 2.1	Band diagram of p-n junction under (a) zero bias and (b) forward bias. Minority carriers diffuse into the neutral regions where they recombine under forward bias conditions [Source: Schubert, 2003a].	<b>18</b>
Figure 2.2	Schematic illustration of (a) non-radiative and (b) radiative transitions in a semiconductor.	<b>19</b>
Figure 2.3	The illustration of electron-hole recombination. The number of recombination events per unit time per unit volume is proportional to the product of electron and hole concentrations.	<b>21</b>
Figure 2.4	The illustration of band diagram of non-radiative recombination (a) via a deep level, (b) via an Auger process and (c) radiative recombination.	<b>22</b>
Figure 2.5a	Schematic of GaN-based LED structure with lateral current path that showed the current crowding problem in a mesa structure GaN-based LED grown on an insulating substrate.	<b>27</b>
Figure 2.5b	Equivalent circuit consisting of n-type and p-type layer resistances, p-type contact resistance, and ideal diodes representing the p-n junction for current flow.	<b>28</b>
Figure 3.1	The mesh creation for (a) coarser and (b) finer mesh for the LED.	<b>38</b>
Figure 3.2	Current-Voltage (I-V) characteristic for coarser and finer mesh creations.	<b>39</b>
Figure 3.3	The cross section at $x = -2.5$ that had been taken throughout the work in order to determine the current, output power and carrier behaviours.	<b>45</b>



Figure 3.4	The flow of simulation procedures.	<b>46</b>
Figure 3.5	The meshed structures of (a) 2D and (b) 3D which shows the difference of grid generation with additional of z-axis that caused the difference in term of results.	<b>47</b>
Figure 3.6	2-D example of Delaunay refinement algorithm [Source: Integrated Systems Engineering, 2003c].	<b>50</b>
Figure 3.7	The output power over active area-current over active area characteristic between 2D and 3D simulations at current over active area of $4 \text{ mA} / \mu\text{m}^2$ . The 2D simulation overestimates the output power over active area at current over active area of $4 \text{ mA} / \mu\text{m}^2$ by nearly 35%.	<b>51</b>
Figure 3.8	The lateral LED structure with thickness values. Inset shows the doping profile of the structure.	<b>52</b>
Figure 3.9	Profile of wavelength for lateral LED structure when approaching 5 V.	<b>53</b>
Figure 4.1	The lateral LED structure with direction of moving anode position, x as the varied applied voltage point of anode for effective length of current path. With similar contact size and fixed cathode position, the distances of anode are varied from the end until it reached the mesa edge. Inset shows the movement of anode positions on p-layer.	<b>55</b>
Figure 4.2	The profile of current and output power as varied applied voltage point along x-axis for lateral LEDs are divided into three zones namely, zone 1, zone 2 and zone 3.	<b>56</b>
Figure 4.3	The ratio of efficiency for conversion of injected current into output power. As varied by applied voltage point for x-axis, the ratio of efficiency is represented by the value of injected output power over current.	<b>58</b>
Figure 4.4	The current density characteristics of different length of current path from 3D structures' cross section when applied voltage point at (a) Sample A, (b) Sample B and (c) Sample C which shows with shorter effective length of current path( $l$ ), the carrier has lower mobility due to the increment number of carriers in the current path.	<b>59</b>
Figure 4.5	The current crowding density behaviour for different applied voltage point at the centre of the device along the y-axis at 5 V.	<b>61</b>

Figure 4.6	The profile of radiative recombination for different applied voltage point at the centre of the device along the y-axis. The inset shows the profile of radiative recombination rate for Sample A at a reduced scale.	<b>62</b>
Figure 4.7	The profile of operating temperature-voltage for different applied voltage points from 2 V to 5 V.	<b>63</b>
Figure 4.8	The plane view of typical LED and modified LED. The dotted arrows in the LED show the possible path for uniform current spreading during LED performance. (a) The typical LED. (b) The modified LED with curved contact edge.	<b>65</b>
Figure 4.9	The 3D view of lateral LED structure with different electrode geometry namely (a) square, (b) hexagonal, (c) octagonal and (d) circular.	<b>66</b>
Figure 4.10	The I-V characteristic of the LED structures with different shape of contacts from 2.5 V to 5 V. Inset shows the calculation for percentage of current and output power performances.	<b>67</b>
Figure 4.11	The L-V characteristic of the LED structures with different shape of contact from 2.5 V to 5 V.	<b>68</b>
Figure 4.12	Current density behaviour of different symmetry shape contact geometrics of (a) square, (b) hexagonal, (c) octagonal and (d) circular.	<b>69</b>
Figure 4.13	The current crowding density behaviour of different electrode geometry in active region at 5 V.	<b>70</b>
Figure 4.14	3D profiles of lattice temperature with different symmetry shape contact geometrics of (a) square, (b) hexagonal, (c) octagonal and (d) circular.	<b>72</b>
Figure 4.15	The radiative recombination rate behaviour of different electrode geometry in active region at 5 V.	<b>73</b>
Figure 4.16	I-V and L-V characteristics of different percentage of contact size area at 5 V.	<b>76</b>
Figure 4.17	Current crowding density profile for 8% and 12% of contact size from top surface area.	<b>77</b>

Figure 4.18	Radiative recombination profile for 8% and 12% contact size from top surface area.	<b>78</b>
Figure 5.1	The profile of current-voltage (I-V) and output power (L-V) for LEDs with slanted mesa sidewall angles.	<b>82</b>
Figure 5.2a	The current density characteristic of different slanted sidewall angles from 3D structures' cross section for over-etched ( $\theta = -18^\circ$ ).	<b>83</b>
Figure 5.2b	The current density characteristic of different slanted sidewall angles from 3D structures' cross section for normal-etched ( $\theta = 0^\circ$ ).	<b>84</b>
Figure 5.2c	The current density characteristic of different slanted sidewall angles from 3D structures' cross section for under-etched ( $\theta = 18^\circ$ ).	<b>84</b>
Figure 5.3	Current crowding profile of over-etched ( $\theta = -18^\circ$ ), normal-etched ( $\theta = 0^\circ$ ) and under-etched ( $\theta = 18^\circ$ ) slanted mesa sidewall angles.	<b>86</b>
Figure 5.4	Radiative recombination profile of over-etched ( $\theta = -18^\circ$ ), normal-etched ( $\theta = 0^\circ$ ) and under-etched ( $\theta = 18^\circ$ ) slanted mesa sidewall angles.	<b>87</b>
Figure 5.5	3D profiles of radiative recombination for (a) over-etched ( $\theta = -18^\circ$ ), (b) normal-etched ( $\theta = 0^\circ$ ) and (c) under-etched ( $\theta = 18^\circ$ ) slanted mesa sidewall angles.	<b>88</b>
Figure 5.6	The measurement of radiation pattern in a circular path around LED at observation radius, R.	<b>89</b>
Figure 5.7a	Polar radiation pattern of selected slanted mesa sidewall from $0^\circ$ to $360^\circ$ observation angles for over-etched ( $\theta = -18^\circ$ ).	<b>90</b>
Figure 5.7b	Polar radiation pattern of selected slanted mesa sidewall from $0^\circ$ to $360^\circ$ observation angles for normal-etched ( $\theta = 0^\circ$ ).	<b>91</b>
Figure 5.7c	Figure 5.6c: Polar radiation pattern of selected slanted mesa sidewall from $0^\circ$ to $360^\circ$ observation angles for under-etched ( $\theta = 18^\circ$ ).	<b>91</b>
Figure 5.8	The pattern of photon reflection profile of selected slanted angle of mesa sidewall (a) over-etched ( $\theta = -18^\circ$ ) and (b) under-etched ( $\theta = 18^\circ$ ).	<b>92</b>

Figure 5.9	Forward I-V characteristics of lateral and vertical LEDs on free standing substrate which shows the superiority of vertical LED performance over lateral LED.	<b>95</b>
Figure 5.10	The output power-voltage (L-V) profile between lateral and vertical configurations on free standing substrate.	<b>96</b>
Figure 5.11a	Current distribution profile of lateral LED configuration with its cross section.	<b>97</b>
Figure 5.11b	Current distribution profile of vertical LED configuration with its cross section.	<b>98</b>
Figure 5.12	The total current density behaviour of different device configurations in active region at 5 V.	<b>99</b>
Figure 5.13	Radiative recombination profile between lateral and vertical configurations.	<b>100</b>
Figure 5.14	The operating temperature-voltage profiles between lateral and vertical configuration at 5 V.	<b>102</b>
Figure 6.1	The structures for future studies (a) partially etched mesa sidewall and (b) ring-shaped etched mesa sidewall.	<b>107</b>

## LIST OF SYMBOLS

$N_D, N_A$	Degrees of concentration donor, acceptor impurities
$w_D$	Depletion region
$V_D$	Diffusion voltage
$D_n, D_p$	Diffusion constant of electron, hole minority carrier
$k$	Boltzmann constant
$T$	Temperature
$e$	Elementary charge
$\mu_n, \mu_p$	Electron, hole minority carrier mobilities
$L_n, L_p$	Electron, hole diffusion length
$\tau_n, \tau_p$	Electron, hole minority carrier lifetime
$E_c, E_v$	Conduction, valence band
$\tau_{nr}, \tau_r$	Non-radiative, radiative recombination lifetime
$n_0, p_0$	Equilibrium electron, hole concentrations
$n_i$	Intrinsic carrier concentration
$p$	Hole concentration
$n$	Electron concentration
$\Delta n, \Delta p$	Excess electron, hole concentration
$B$	Bimolecular coefficient
$R$	Recombination rate per unit time per unit volume
$E_T$	Non-radiative recombination rate through a deep level with trap energy
$N_T$	Carrier concentration at energy trap level
$E_{Fi}$	Fermi level in the intrinsic semiconductor
$R_{SR}$	Shockley, Read and Hall recombination model
$v_n, v_p$	Electron, hole thermal velocities
$\sigma_n, \sigma_p$	Capture cross sections of the traps
$n_1, p_1$	Electron, hole concentrations if the Fermi energy is located at the trap level
$E_g$	Energy gap
$\tau$	Total probability of recombination
$R_r, R_{nr}$	Radiative, non-radiative recombination rate

$n_{int}$	Probability of radiative recombination or internal quantum efficiency
$t_n$	Thickness of the n-type layer
$t_p$	Thickness of the p-type layer
$w$	Width of the LED structure
$x$	Position along the $x$ direction
$V$	Voltage
$\rho_n$	Resistivity of the n-type layer
$I_o$	Diode saturation current
$V_j$	Voltage drop across the active region
$R_v$	Vertical resistance
$\rho_c$	P-type specific contact resistance
$J_o$	Current density at the p-type contact edge
$\rho_p$	Resistivity of the p-type cladding layer
$J$	Current density
$L_s$	Current spreading length
$L_t$	Current transfer length
$R_n$	The resistances inside the n-type layer
$R_p$	P-type layer resistance
$R_c$	P-type contact resistance resistance
$n_{i, eff}$	Effective intrinsic density

## LIST OF ABBREVIATIONS

LED	Light Emitting Diode
OLED	Organic Light Emitting Diode
GaN	Gallium Nitride
SiC	Silicon Carbide
2D	Two Dimensional
3D	Three Dimensional
ISE TCAD	Integrated Systems Engineering Technology Computer-Aided Design
InGaN	Indium Gallium Nitride
GUI	Graphical User Interface
UV	Ultraviolet

**SIMULASI KE ATAS PRESTASI DIOD PEMANCAR CAHAYA  
BERASASKAN GaN DENGAN KEPELBAGAIAN GEOMETRI DAN  
REKABENTUK SENTUHAN**

**ABSTRAK**

Objektif utama kajian ini adalah untuk meminimumkan masalah kesesakan arus yang berlaku pada diod pemancar cahaya (LED) yang berasaskan GaN. Kesesakan arus akan menyebabkan pemanasan sendiri dan rekombinasi radiatif yang menyekat potensi sebenar LED yang berprestasi tinggi dari segi elektrik dan optikal. Dengan menggunakan simulator peranti, ISE TCAD sebagai alatan, masalah kesesakan arus dikaji pada pelbagai struktur geometri p-i-n LED sentuhan sisi. Laluan arus sisi yang efektif di antara dua sentuhan diperiksa dengan menetapkan kedudukan sentuhan n manakala sentuhan p dilaras atas lapisan p. Kajian ini mendedahkan bahawa kedudukan sentuhan p pada tengah lapisan jenis p adalah laluan arus sisi yang efektif di mana terdapat taburan arus yang seragam dan rintangan sesiri yang rendah disebabkan oleh jarak penyebaran pergerakan pembawa yang simetri. Berdasarkan laluan arus sisi yang efektif, kesan geometri sentuhan menunjukkan prestasi bentuk sentuhan segiempat mengatasi bentuk yang lain iaitu heksagon, oktagon dan bulatan. Bentuk segiempat yang mempunyai kawasan lilitan sentuhan yang terbesar membantu arus untuk tersebar secara seragam dan mengurangkan potensi kesesakan arus pada sentuhan n disebabkan oleh rintangan yang rendah sepanjang laluan arus. Kajian dilanjutkan ke atas pengaruh saiz kawasan sentuhan untuk mengesahkan penemuan dalam kajian geometri sentuhan. Had saiz sentuhan tertentu dikenakan apabila kita cuba untuk mengoptimumkan kawasan suntikan arus kerana saiz sentuhan yang besar akan mengurangkan kuasa output



disebabkan rekombinasi tidak radiatif. Kebarangkalian cahaya untuk memancar juga meningkat apabila dinding tepi mesa struktur LED sisi dicondongkan kerana foton dipesongkan pada sudut condong bergabung dengan foton yang dipancar oleh permukaan secara langsung. Akhir sekali, perbandingan antara struktur LED sentuhan sisi dan sentuhan tegak dibuat untuk mengukur tahap masalah kesesakan arus dan penyelerakan haba pada struktur kajian.

# **SIMULATION ON PERFORMANCE OF GaN-BASED LIGHT EMITTING DIODES WITH VARIED GEOMETRY AND CONTACTS DESIGN**

## **ABSTRACT**

The main objective of this research is to minimize the current crowding problem inside GaN-based Light Emitting Diode (LED). Self heating effects and low radiative recombination are among the consequences that restrict the true potential of high electrical and optical performance of LED. By using device simulator, ISE TCAD as a tool, current crowding problem is investigated with varied geometries of lateral p-i-n LED structure. The effective lateral current paths between two contacts are examined by fixing the position of n-contact while p-contact position is varied on p-layer. This work revealed that the location of p-contact at the centre of p-type layer was the effective length of lateral current path where better current distribution and low series resistance were obtained due to the symmetry of current spreading length for carrier movement. Based on the effective lateral current path, the effect of contact geometrics showed that square shape contact out-performed other shape, namely hexagonal, octagonal and circular. The square shape which has largest contact periphery area helped current to spread uniformly and reduces the potential of current crowding at the n-contact due to lower resistance along the current path. Extended investigation on the influence of contact area size is carried out to verify previous findings in contact geometrics study. Certain limitations of the contact size is applied when we try to optimize the current injected area since bigger contact size will lower output power due to non-radiative recombination. The possibility of emitted light also increased when the mesa sidewall of lateral LED structure is slanted since the deflected photons at the slanted angle will combine with direct

surface-emitting photons. Lastly, comparison between lateral contact and vertical contact LED structures is made to quantify the height of current crowding problem and heat dissipation of studied structures.

# CHAPTER 1

## INTRODUCTION

### 1.1 Light Emitting Diode (LED)

Electroluminescence phenomenon, accidentally discovered by Henry Joseph Round (1907) was the starting point for the emergence of light emitting diodes or LEDs. However, the effect was not understood until 1951 when Lehocvec explained the radiative recombination of electrons and holes as a result of injection of minority carriers across a forward biased p-n junction (Lhocvec *et al.*, 1951), after the invention of the p-n junction in 1947. Numerous studies were carried out, starting by Hayness *et al.*, 1952 and Wolff *et al.*, 1955 since then and different materials were found capable of producing visible light emitters. The awareness of potential replacement for light bulbs as light sources also grown tremendously since then and the interest in this area led to intensive investigation on it.

Even though at present incandescent bulb lamps and fluorescent lamps are used as light sources for many applications, their poor reliability and durability and low luminous efficiency shortened their potential for future general illuminator. These conventional and traditional glass-vacuum-type light sources are heavily dependent on either incandescence or discharge gases to operate. Most of their energy are converted into heat instead of light and indirectly contributed to global warming problem by reducing the green-house gases. Therefore, next generation light sources such as LEDs are very indispensable to stabilize the environment issues while maintaining the quality of light that we deserved.

Recent breakthrough in solid-state lightning has made LEDs as the front runner to become the dominant light source in the future. State-of-the art LEDs are small, rugged, reliable, bright, and efficient thanks to their rapid development in recent years. Moreover, their higher reliability, longer lifetime and lower power consumption attributes made them superior to their predecessors. The profile of LEDs rapid development is shown in Figure 1.1. Despite the humble beginnings, LEDs acquired high importance within a relatively short time. Recent studies have demonstrated 117 lumens per watt (lm/ W) in white GaN-based LEDs, with further improvements expected in the near future (Nakamura, 2009).

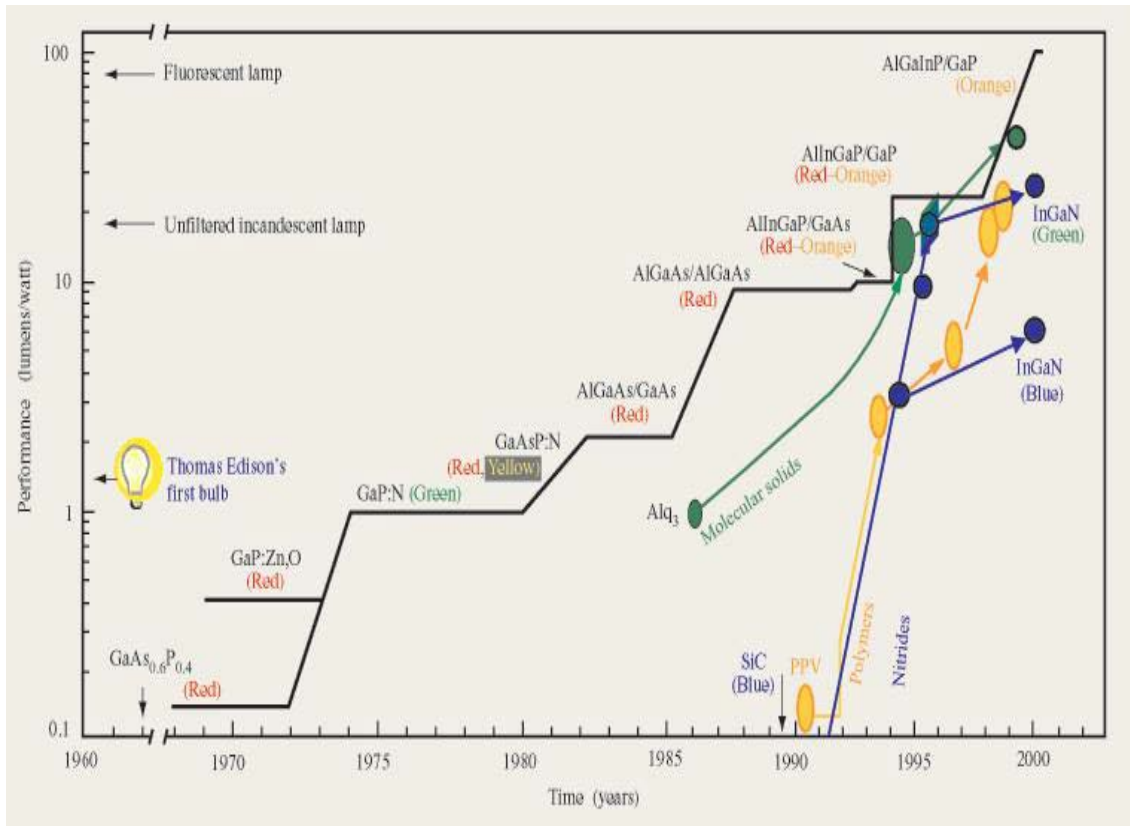


Figure 1.1: Evolution of LED and organic LED (OLED) performance (Source: Sheats *et al.*, 1996).

The advancement in material science also accelerated the development of LEDs. LEDs are highly monochromatic, emitting a pure color in a narrow frequency range. With various energy bandgap, LEDs could produce the different wavelength of light and this potential could be optimized by doing material engineering processes on the structures. A range of wavelength spectrum from ultraviolet to infrared can be obtained by selected materials which could emit light when electroluminescence effect takes place.

Currently, the potential applications of LEDs in areas such as full-color indicators, full-color displays and high-efficiency lamps are among the motivations for researchers and manufacturers to invest their time and money on this cold light sources. The combination of three primary colors, namely red, green, and blue, which could be obtained from the solid-state LEDs can reproduce the visible color spectrum that are crucial to fulfill their promising potential. Apart from that, other application of LEDs in areas such as remote control and optical communication applied their non-visible light and proved its versatility compared to conventional lamps.

## **1.2 Gallium Nitride (GaN) based LED**

The development of nitride semiconductors opened the way to obtain all-solid-state semiconductor light sources. The ability of GaN-based LEDs to be used as one of three LEDs to tune to any color in the visible range, or even use a single blue LED in combination with phosphors to make ‘white LEDs’ are very attractive for next generation illuminator. Furthermore, the short wavelength which is produced by GaN-based LEDs has increased the number of data that would be transferred in optical communication. Therefore, by decreasing costs and increasing the performance of

LEDs we can expect more economical, more reliable and longer lifetime illumination in the future.

The p-type doping breakthroughs opened the door for efficient p-n junction LEDs and laser diodes. The reported works of the first p-n homojunction LED (Akasaki *et al.*) and first viable blue and green GaN-based LEDs (Nakamura *et al.*, 1993a; Nakamura *et al.*, 1993b; Nakamura *et al.*, 1994) were a turning point for advancement of GaN-based LEDs after work on GaN virtually ceased. Several remarkable physical properties make the group-III nitrides attractive for reliable solid-state device applications. The wide bandgap materials possess low dielectric constants with high thermal conductivity pathways and it allows for high quantum efficiency light emitters to be fabricated. Furthermore, the GaN-based LEDs can operate under harsh environments due to their high bond strengths and very high melting temperatures. Thus, these properties may lead to LEDs with superior reliability.

### **1.3 Geometrical Design Issues On Lateral GaN-Based LEDs Performance**

The issues of appropriate substrates for GaN-based LEDs slowed down its development since several problems in the epitaxial growth of nitrides originate from the non-availability of single crystalline GaN substrates or other high quality single crystalline substrates with the same lattice parameters as GaN. For this reason, most of the epitaxial growth of nitrides has been performed on sapphire or Silicon Carbide (SiC) as good substrates for the time being.

Since sapphire is insulating while SiC is conducting substrates, the differences in term of current injection types inside LEDs for both substrates are expected with LEDs that used sapphire as substrate employs a lateral device configuration while the one with

SiC substrate employs vertical device configuration. Both of the configurations have their own advantages and drawbacks that need to be considered in order to study the effects of geometrical design on LEDs performance.

Generally, LEDs on sapphire substrates are fabricated in a lateral device configuration which both n and p type electrodes need to be located on the top side of the epitaxial structure due to the insulating substrate. The use of insulating sapphire substrates have several drawbacks such as lattice mismatch between sapphire and III nitrides, poor thermal conductivity and current crowding problem at the edge of the mesa edge that is near to the n-type contact. Compared to sapphire, SiC enables vertically structured LEDs with a top p contact and a bottom n contact due to the conducting substrate. However, similar to LEDs on sapphire, the lattice mismatch between SiC and III nitrides results in a large number of dislocations in the device structure. Besides, high series resistance due in part to the resistive buffer layer ( Edmond *et al.*, 1997 ) and the absorption of light by substrates also decrease the LED efficiency.

At the same time, the cost effective and high performance LEDs are among of the main criteria that will determine the type of substrates. Currently, most of commercially available and extensive research study about GaN-based LEDs are conducted on LEDs that were grown on insulating sapphire substrates due to cost and transparency to light extraction as compared to conductive SiC substrates. Based on the current development, the studies related on the performance of GaN-based LEDs on sapphire are widely discussed. The issues regarding to current crowding problem is one of main problems that need to be addressed in order to optimize the LEDs performance.



For this reason, the understanding on the current crowding issue will lead to achieving that objective.

Generally, LEDs performance has been greatly improved by materials growth, materials systems, structures and better contacts (Kim *et al.*, 2000a; Zukauskas *et al.*, 2002; Steigerwald, 2002; Brown *et al.*, 2003). As progress in material issues is quickly being saturated, the possibility to develop high-brightness and high-efficiency LEDs are explored into the geometrical issues. The fact that most of GaN-based LEDs have a critical weakness in its fabrication which mainly involves the use of lateral carrier injection type due to the absence of appropriate conducting substrates make this study become more interesting. Due to the lateral device configuration, current crowding problem is often encountered and impedes the development of the efficient GaN-based LEDs. Therefore, novel contact and device geometries studies are introduced in order to alleviate the current crowding problem.

Previously, Eliashevich *et al.*, 1999, demonstrated theoretically and experimentally, that the conductivity of n-type GaN layer has a profound effect on uniform current spreading. Their current spreading model assumed the transparent metal layer to be a perfect current spreader where metal conducting layer have a negligible resistance. It is noted that the uniform current spreading is essentially attained above the critical n-type carrier concentration. Furthermore, the nonuniform current spreading could significantly degrade the properties of LED performance due to the current crowding in a localized region of the device. Later, more highly developed theoretical model has been proposed and important parameters such as the current density, the resistivities of the transparent electrode and n-type layers, and the effective length for the lateral current path were found to be important factors in uniform current spreading.

Kim *et al.*, 2000a and Kim *et al.*, 2000b, showed that LED lifetime decrease significantly with increasing value of current density, which can only be attributed to nonuniform current spreading. Their modified model take into account the contribution of resistance from metal layer which explained the problem of localized current crowding that degrade device lifetime encountered in experimental work. Figure 1.2 compares a typical LED (a) and the added extra pad at p-type LED (b). Thus, by adding an extra p-type pad, the length of the lateral current path through the transparent layer is reduced and LED performance improved.

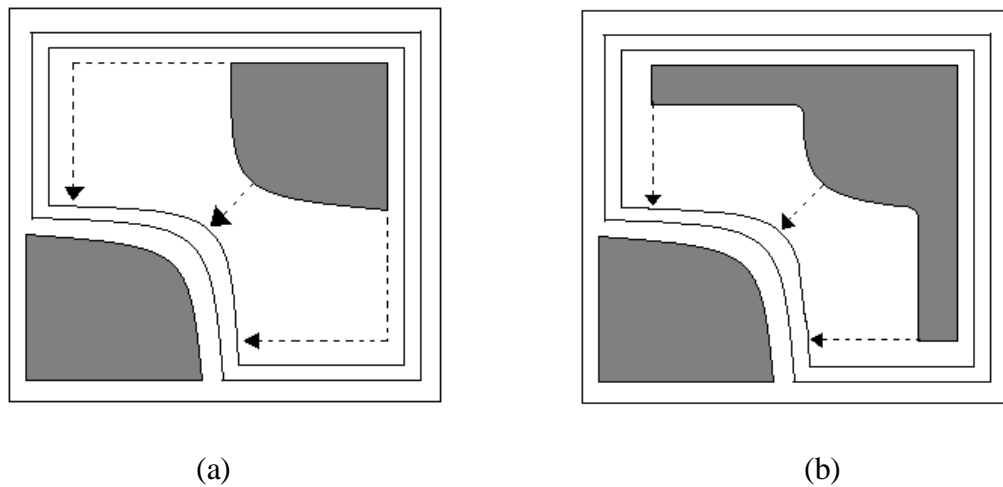


Figure 1.2: The plane view of typical LED and modified LED. The dotted arrows in the LED show the possible path for uniform current spreading during LED performance. (a) the typical LED. (b) the modified LED with extra pad at p-type.

Further investigation by Kim *et al.*, 2001a proposed that two important parameters; applied current density and the effective length for the lateral current path, significantly affect the performance of LEDs. In this study, modification of the p-type electrode geometry based on the effective length factor contributed to significant improvements in LED characteristics due to uniform current distribution. Meanwhile,

other study by Jin *et al.*, 2000 proved that the increment of the LED performance in term of geometrical design issues is not really significant to minimize the current spreading problem. However, the geometrical design such as the interconnected microdisk LED that they investigated showed a 60% increase in optical emission efficiency compared to the conventional broad-area LED.

The emergence of novel geometrical LED design such as ring-shaped mesa geometry had reduced current crowding problem unlike those in LEDs employing the conventional square-shaped mesa geometry (Guo and Shubert, 2001a). Even though both geometries experienced the optical saturation effects, the LED with ring shaped p-type mesa had less optical saturation effects due to shorter length of current flow in the n-type layer and more mesa wall surface which improved light extraction efficiency towards lateral directions. A quantitative model of current crowding also revealed an exponential decrease of the current density with respect to distance from the mesa edge. The current crowding near the edge of the contact was attributed to finite resistance of n-type GaN layer according to their model (Guo and Shubert, 2001a).

Later on, Guo *et al.*, 2001b, had proposed a different mode for efficiency enhancement; an interdigitated mesa. The performance of the design generally improved due to more uniform current distribution and larger mesa sidewall area for better light extraction. Other study revealed that the interdigitated designs are scalable and can be used in high power, large-area devices (Krames *et al.*, 2000). This geometrical design is more scalable than the traditional square-shaped geometry especially for large die LEDs that are normally affected from current crowding near the mesa edge. The traditional square-shaped geometry LEDs has a higher possibility to absorb its emitted light inside the device since the light has to travel in longer length. Thus by designing appropriate

width of contact fingers for the interdigitated geometry, light travel length toward the side finger can be kept as small as in small die size devices.

Further numerical analysis conducted on more complicated interdigitated geometry as shown in Figure 1.3 revealed the current crowding effect near n or p pads according to the lateral current injection. The model which included the resistance component of the p-type transparent electrode showed a reduction of the lateral mesa length which increases the current injection efficiency based on their exponential behaviour as a function of the lateral length (Kim *et al.*, 2001b and Kim *et al.*, 2002). Other studies conducted by Ebong *et al.*, 2003 use the Aimspace device and circuit simulator. Their uniform current spreading model showed that a strong correlation on LED designs as well as p-transparent metal contact and n-GaN layer resistivity. Ebong *et al.* noted that LED design which has the symmetry in the current spreading length exhibited better current distribution and current uniformity is a function of contact resistance.

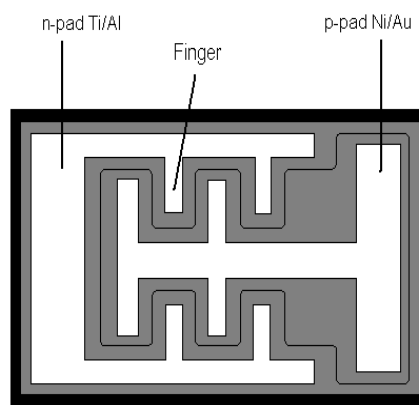


Figure 1.3: The geometry of interdigitated geometry LED.

Recent work on nanometer scaled GaN-based LEDs promised more options to optimize the potential of LEDs (Jin *et al.*, 2000; Choi *et al.*, 2003a; Choi *et al.*, 2003b and Choi *et al.*, 2005). As revealed by Choi *et al.*, 2004, the design of this LED type as shown in Figure 1.4 increased the surface area for light extraction and minimized losses due to internal reflection and reabsorption. Based on their results, Choi *et al.*, 2004 noted that the microring emit more light to the detector at a wide range of injection currents. Furthermore, their large surfaces are played an important role of heat sinking which made them suitable for operation at high currents.

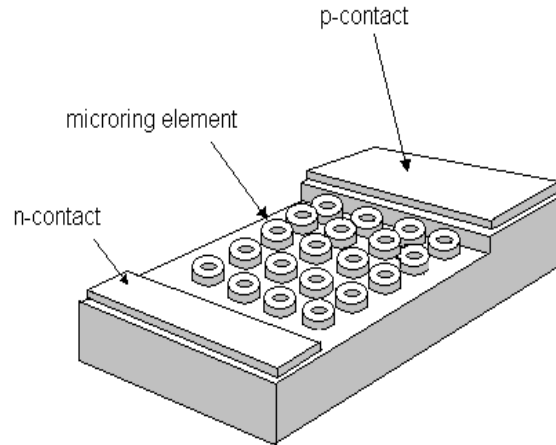


Figure 1.4: The geometry of microring LED.

As interest of nano-scale geometrical modification LEDs design increased, studies on the effects on the device surface also grow in recent years. Numerous works on the contribution of mesa sidewall illumination in order to increase the LED efficiency are conducted (Lin *et al.*, 2005; Yu *et al.*, 2006; Huang *et al.*, 2006 and Lee *et al.*, 2006). The factor that certain degrees of mesa sidewall arrangement could enhance the light extraction efficiency while reducing current crowding problem is very appealing for researchers to investigate and optimize the LEDs performance. The large difference in

the refractive index between the semiconductor and the air lead to low external quantum efficiency (Pan *et al.*, 2003 and Chang *et al.*, 2004). The significant gap existed between the internal quantum efficiency and external quantum efficiency of LEDs due to difference of refractive index need to be reduced. Therefore, several works will be carried out to reveal the importance of geometrical designs on device efficiency based on the current development of LEDs design in order to minimize the current crowding problem.

#### **1.4 The advancement of simulation**

The availability of software tools for device modeling in recent years accelerated the LED manufacturing technology. Typically, manufacturing alone is a very costly and slow process. However, with robust modeling technology, the design of high performance LEDs could omit several steps such as design, manufacture and characterize actual LED devices which need to be repeated before optimizing the devices. Thus, by implementing the simulation procedures we could improve design characteristics and overall performance of LEDs much quicker and cheaper than fabricate it from scratch.

Apart from that, several phenomenons are hard to monitor and measure in the fabrication process due to nano-scale structures. Generally, most of the simulation works are based on two dimensional (2D) structures (Bulashevich *et al.*, 2006 and Soohwan *et al.*, 2006). However, recent breakthrough in the three dimensional (3D) simulation offers more reliable and more realistic way to study about the effect of nano-scale differences in physical appearance especially the geometry of LED which is otherwise difficult to determine by fabrication. Numerous 3D simulation works (Piprek *et al.*, 2004; Li *et al.*,

2006 and Sheng *et al.*, 2007) suggest the beneficial influence on the development of LED performance.

As predictive tool, the user of simulation can get the general ideas about the device performance and its mechanism which is related to the theoretical knowledge of semiconductor devices. Furthermore, the graphical information from the simulated device shows what actually happens inside the device. Therefore, with robust modeling technology, a growing number of expensive and time-consuming experimental works can be more efficient in order to accelerate the LEDs development.

In this project, 3D structures of LED are numerically investigated by using ISE TCAD (Integrated Systems Engineering Technology Computer-Aided Design) simulation software. Only active area of LED structure which is mainly contributing for emission efficiency of LEDs is simulated in order to reduce the time consumption while maximizing the LED performance. These integrated tools are used to investigate the electrical and optical properties of the device when various geometrical modifications are made on the device.

## **1.5 The research objective**

The main objective of this research is to minimize current crowding problem in LED through design of device geometry by using a device simulator as a tool. To achieve the main objectives, several sub objectives has been identified:

1. To study the effective lateral current path between two contacts on LED performance.
2. To study the effects of contact geometry on LED performance.
3. To study the effects of contact size area on LED performance.

4. To study the effects of slanted mesa sidewall on LED performance.
5. To study the difference between lateral and vertical configurations on LED performance.

All of the sub objectives need to consider the current path since both n and p type electrodes of GaN-based LEDs are located on the top side of the epitaxial structure due to the insulating substrate. Thus, by investigating the effective current path for each one of them will lead us to achieving the main objective which is to minimize current crowding problem and indirectly enhanced the LEDs electrical and optical performance.

## **1.6 Outline of Thesis**

In brief, the contents in this thesis are arranged as follows:

Chapter 2 covers the related theories and concepts about device that are relevant to the work in this research.

Chapter 3 explains the simulator itself and simulation procedures that are involved in this work. These procedures briefly describe several selected models used in the simulation.

Chapter 4 presents the results from this research work. The LED performance on various geometrical designs that are related to contact geometrics are presented, analyzed and discussed.

Chapter 5 presents the results and discussions of an extended investigation on the effects of mesa sidewall on LED performance.



Chapter 6 concludes the thesis with a summary of the research work. Conclusions of the results are made and a few suggestions for future research are included.

## CHAPTER 2

### THEORY OF LED

#### 2.1 Introduction

This chapter discusses about the overview of LED theory. Basic principles of LED in terms of electrical and optical properties are presented. Discussion from literature reviewed the main problem; current crowding and its theory related to geometrical design of GaN-based LEDs on sapphire substrate are also presented.

#### 2.2 Principle of LED

LED is a class of diodes that emit spontaneous radiation under suitable forward bias conditions. The basic LED consists of p-n junction that is fabricated from semiconductor materials. Injection electroluminescence is the most important mechanism to excite the carriers inside semiconductor to produce the light. Under forward bias conditions, light can be created when an electron injected into a p-type semiconductor radiatively recombines with a hole, or when a hole injected into n-type semiconductor radiatively recombines with an electron. Like normal diode, current will flow in one direction across the junction when both of these materials are connected with contacts on each end.

In order to create the p-n junction, both p and n types of semiconductor material are doped with impurities. The n-type semiconductor is doped with certain degrees of concentration donor impurities,  $N_D$  while p-type semiconductor is doped with certain degrees of concentration acceptor impurities,  $N_A$ . These dopants create the gradient of carrier concentration at the vicinity of an unbiased p-n junction. Under equilibrium

condition, electrons originating from donor on the n-type side diffuse over to the p-side where they encounter many holes with which they recombine. A corresponding process occurs with holes that diffuse to the n-type side.

As electrons diffuse from the n region, positively charged donor atoms are left behind. Similarly, as holes diffuse from the p region, they uncover negatively charged acceptor atoms. The net positive and negative charged regions in the n and p regions induce an electric field that essentially swept all electrons and holes out of the regions unless external bias voltage is applied. These two regions are referred to as space charge region due to the phenomenon. Since the space charge is depleted of any free carriers, this region is also referred to as the depletion region,  $w_D$  as shown in Figure 2.1 (a). These two terms are used interchangeably.

At the same time, space charge region also produce a potential or barrier that is called the diffusion voltage,  $V_D$  where free carriers must overcome in order to reach the neutral region of opposite conductivity type. In homojunction LEDs, where the p-type and n-type regions are composed of the same energy gap semiconductor material, the carrier distribution is largely dependent on the diffusion constant. However, the diffusion constant of carriers is not easily measured. Thus, the carrier mobility by the Hall effect is used in order to infer the diffusion constant by using the Einstein relation which is given by

$$D_n = \frac{kT}{e} \mu_n \quad \text{and} \quad D_p = \frac{kT}{e} \mu_p \quad (2.1)$$

where  $D_n$  is diffusion constant of electron minority carrier,  $D_p$  is diffusion constant of hole minority carrier,  $k$  is Boltzmann constant,  $T$  is temperature,  $e$  is elementary charge,

$\mu_n$  and  $\mu_p$  are electron and hole minority carrier mobilities. This equation is only applied for non-degenerate semiconductor. Without external electric field applied, carriers injected into a neutral semiconductor are propagating by diffusion.

When external bias applied, p-n junction barrier decreases or increases according to the type of bias whether it is forward or reverse bias, respectively. The voltage is going to drop across the depletion region with the application of bias voltage to the p-n junction. Under forward bias conditions where n-type region and p-type region of diode are connected to negative and positive side of electrical circuit, respectively, electrons and holes are injected into the region with opposite conductivity type and current flow increases. The diffusion of carriers into the regions of opposite conductivity type enable minority carriers to recombine and emit a photon.

Before the recombination, the minority carriers have to diffuse at certain distance which is called diffusion length. On average, electrons injected into p-type region will diffuse over the diffusion length  $L_n$  before recombining with holes. A corresponding process occurs with holes that diffuse to the n-type side. The diffusion length is given by

$$L_n = \sqrt{D_n \tau_n} \quad \text{and} \quad L_p = \sqrt{D_p \tau_p} \quad (2.2)$$

where  $\tau_n$  and  $\tau_p$  are electron and hole minority carrier lifetime, respectively.

In Figure 2.1 (b), the distribution of carriers in p-n junction under forward bias with diffusion length and lifetime is shown. Based on the figure, note that the minority carriers are distributed over a large distance while minority carrier concentration decreases as these carriers diffuse further into the adjacent region. Therefore, the

recombination process occurs over a large region with a strongly changing minority carrier concentration. However, the large recombination region in homojunction is not worthwhile for efficient recombination.

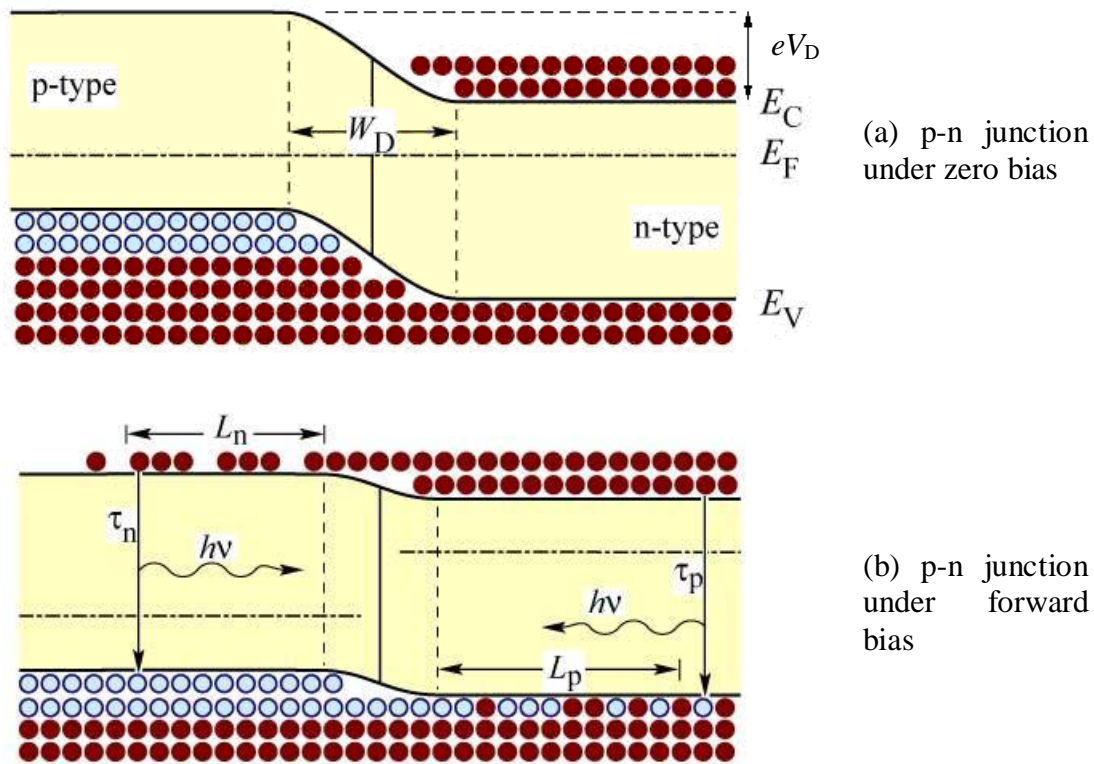


Figure 2.1: Band diagram of p-n junction under (a) zero bias and (b) forward bias. Minority carriers diffuse into the neutral regions where they recombine under forward bias conditions (Source: Schubert, 2003a).

### 2.3 Radiative and non-radiative recombination

Generally, electron-hole recombination can be either radiative or non-radiative. These two recombination pathways can be considered as parallel processes occurring across the energy bandgap of the semiconductor as shown in Figure 2.2. In light emitting devices, the radiative recombination is clearly a preferred process. Light output from LED can be increased by maximizing the probability for radiative recombination while

decreasing the probability for non-radiative recombination. In other words, there is competition between radiative and non-radiative recombination which should be won by radiative recombination in order to obtain the light emission.

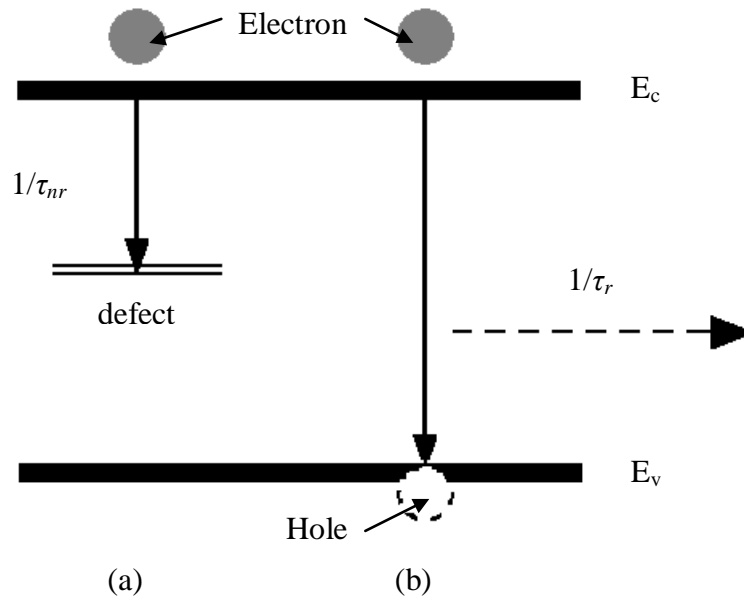


Figure 2.2: Schematic illustration of (a) non-radiative and (b) radiative transitions in a semiconductor.

Primarily, the radiative transitions in semiconductor occur by interband transitions, excitonic recombination, or recombination through impurity centres. As mentioned before, the released energy is emitted as electromagnetic radiation in a radiative recombination process. Meanwhile, several mechanisms cause non-radiative recombination in semiconductor, among these are; Auger recombination, recombination at defect sites, and multiphonon emission at deep impurity sites (Henry *et al.*, 1976). Contrast to radiative recombination process, there is no radiation emitted and the released energy is eventually converted to thermal energy in the form of lattice vibrations in a non-radiative recombination process.

### 2.3.1 Radiative electron-hole recombination

As known, any undoped and doped semiconductor has two types of free carriers, namely electrons and holes. Under equilibrium conditions which is no external influences such as light or current, the product of the electron and hole concentrations at a given temperature, is given as

$$n_o p_o = n_i^2 \quad (2.3)$$

where  $n_o$  and  $p_o$  are the equilibrium electron and hole concentrations and  $n_i$  is the intrinsic carrier concentration.

Meanwhile, the excess carriers can be generated in semiconductor when the external influences either absorption of light or current injection is applied. The total carrier concentration is then given by the sum of equilibrium and excess carrier concentration as

$$n = n_o + \Delta n \quad \text{and} \quad p = p_o + \Delta p \quad (2.4)$$

where  $\Delta n$  and  $\Delta p$  are the excess electron and hole concentration, respectively.

The illustration of band diagram of a semiconductor with electrons and holes as shown in Figure 2.3 helps the explanation about the recombination of carriers. In this explanation, recombination rate is denoted as  $R$  and a free electron in the conduction band is considered. The probability that the electron recombines with a hole is proportional to the hole concentration,  $R \propto p$  while the number of recombination events will also be proportional to the concentration of electrons,  $R \propto n$ . It could be concluded that the recombination rate is proportional to the product of electron and hole concentrations,  $R \propto n p$ .

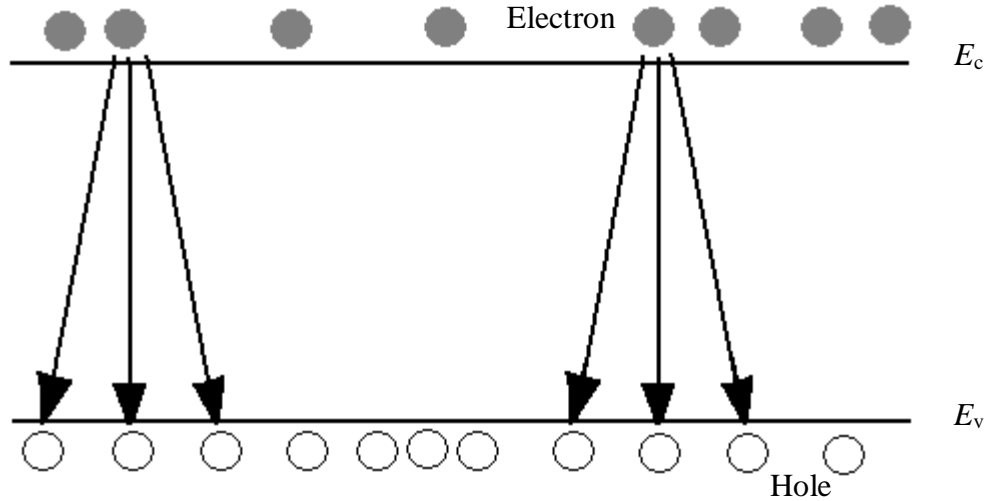


Figure 2.3: The illustration of electron-hole recombination. The number of recombination events per unit time per unit volume is proportional to the product of electron and hole concentrations.

By using a proportionality constant, the recombination rate per unit time per unit volume can be indicated as

$$R = -\frac{dn}{dt} = -\frac{dp}{dt} = Bnp \quad (2.5)$$

where the proportionality constant  $B$  is called the bimolecular coefficient. This equation is known as bimolecular rate equation. Typically,  $B$  value for III-V semiconductors is in range of  $10^{-11}$  to  $10^{-9}$   $\text{cm}^3/\text{s}$ .

### 2.3.2 Non-radiative electron-hole recombination

As previously mentioned, non-radiative recombination events are unwanted in LEDs since the electron energy is converted to vibrational energy of lattice atoms. In other word, the recombination generates heat which would degrade the performance and



lifetime of the device. There are several physical mechanism by which non-radiative recombination can occur such as in the bulk and at the surfaces of semiconductor. Commonly, defects in crystal structure are the cause for non-radiative recombination in the bulk of semiconductor which include unwanted foreign atoms, native defects, dislocations and any complexes of defects, foreign atoms or dislocations. Meanwhile, native defects include interstitials, vacancies and antisite defects in compound semiconductor (Longini and Greene, 1956; Baraff and Schluter, 1985).

In term of energy levels, all defects have their own energy level structures that are different from substitutional semiconductor atoms. Thus, there are probabilities that each defects to form one or several energy levels within the forbidden gap of semiconductor. Generally, energy levels within the gap of the semiconductor are efficient recombination centres especially if the energy level is close to the middle of the gap. However, in this case the recombination promotes the non-radiative processes such deep levels or traps which also known as luminescence killers. The recombination of carriers via a deep level is shown in Figure 2.4 (a).

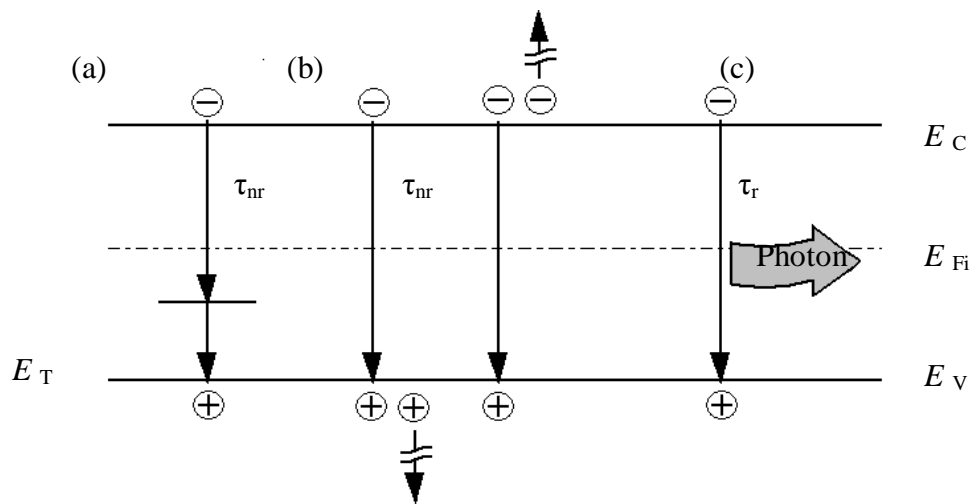


Figure 2.4: The illustration of band diagram of non-radiative recombination (a) via a deep level, (b) via an Auger process and (c) radiative recombination.

The non-radiative recombination rate through a deep level with trap energy,  $E_T$  with concentration,  $N_T$  which was first analyzed by Shockley, Read and Hall (Hall, 1952; Schockley and Read, 1952) is given as

$$R_{SR} = \frac{p_o \Delta n + n_o \Delta p + \Delta n \Delta p}{(N_T v_p \sigma_p)^{-1} (n_o + n_1 + \Delta n) + (N_T v_n \sigma_n)^{-1} (p_o + p_1 + \Delta p)} \quad (2.6)$$

where  $\Delta n = \Delta p$ ,  $v_n$  and  $v_p$  are the electron and hole thermal velocities, while  $\sigma_n$  and  $\sigma_p$  are the capture cross sections of the traps. Form the equation 2.6, the quantities  $n_1$  and  $p_1$  are the electron and hole concentrations if the Fermi energy is located at the trap level.

These quantities are given by

$$n_1 = n_i \exp\left(\frac{E_T - E_{Fi}}{kT}\right) \quad \text{and} \quad p_1 = n_i \exp\left(\frac{E_{Fi} - E_T}{kT}\right) \quad (2.7)$$

where  $E_{Fi}$  is the Fermi level in the intrinsic semiconductor.

Meanwhile, Auger recombination is another important non-radiative recombination mechanism that occurred in bulk of semiconductor. In this process, a free electron is excited high into the conduction band or hole is excited deeply into the valence band due to the dissipation of available energy obtained through electron-hole recombination, approximately  $E_g$ . The highly excited carriers will subsequently lose energy by multiple phonon emission until they are close to the band edge. The mentioned processes are illustrated in Figure 2.4 (b). However, the Auger recombination rate is very small and can be neglected at lower carrier concentrations or

lower excitation intensity for practical purposes due to the cubic carrier concentration dependence.

Apart from that, substantial non-radiative recombination also can occur at semiconductor surfaces. Based on the strict periodicity of a lattice in band diagram model, surfaces are a strong perturbation of the periodicity of a crystal lattice. The band diagram will need to be modified at a semiconductor surface since the periodicity ends at a surface. The addition of electronic states within the forbidden gap of the semiconductor is one of the effects that appear due to the modification. The electronic states play their role as recombination centres within the forbidden gap (Shockley, 1950).

However, the surface recombination can occur only when both types of carriers are present. Thus, the carrier-injected active region in which naturally both types of carriers are present should be kept away from the surface at several diffusion lengths to minimize the surface recombination. In order to achieve that motivation, the arrangement of contact that are sufficiently far away from the side surfaces of the die with smaller current injection under a contact than semiconductor die is among the solutions that can be done to reduce the possibility of that non-radiative recombination. The carriers will not 'see' any semiconductor surfaces if the current flow is confined to the region below the contact. It shown that surface recombination can be drastically reduced by device designs that spatially separate the active region from any surfaces. However, few carriers will still diffuse to the surface and recombine there even if the separation is large.